

Article

Effect of La Addition on Microstructure and Properties of Al-0.2Fe-0.06Cu Alloy

Yawu Xu ¹, Zixuan Peng ¹, Dongyan Ding ^{1,*} , Wenlong Zhang ¹, Yongjin Gao ², Guozhen Chen ², Yonglin Xie ² and Yongqi Liao ²

¹ School of Materials Science and Engineering, Shanghai Jiao Tong University, Shanghai 200240, China; xu1234@sjtu.edu.cn (Y.X.); pengzixuan@sjtu.edu.cn (Z.P.); zhangwl@sjtu.edu.cn (W.Z.)

² SJTU-Huaafon Joint Lab, Shanghai Huaafon Al Co., Ltd., Shanghai 201506, China; gao.yongjin@huaafeng.com (Y.G.); chen.guozhen@huaafeng.com (G.C.); xie.yonglin@huaafeng.com (Y.X.); liao.yongqi@huaafeng.com (Y.L.)

* Correspondence: dyding@sjtu.edu.cn; Tel.: +86-21-3420-2741

Abstract: The increasing application of lithium-ion batteries has led to higher requirements being imposed on the performance of current collectors. In this work, the effect of La content on the microstructure and properties of Al-0.2Fe-0.06Cu alloy was investigated through optical microscopy, scanning electron microscopy and mechanical/electrical/electrochemical performance tests. Experimental results indicated that the addition of La was beneficial to grain refinement and promote the formation of La-containing compounds. However, excessive La addition weakened the refinement effect. Grain refinement played a major role in affecting the mechanical properties of the alloy, but had little effect on the conductivity. In comparison with Al-0.2Fe-0.06Cu, the La-containing alloys had lower corrosion potential, which indicated that the addition of La element could improve the corrosion resistance of the Al-0.2Fe-0.06Cu alloy. The addition of La improved the mechanical properties of the alloy at room temperature and 50 °C. When the La addition was 0.1wt.%, the alloy had the best mechanical properties. The corrosion resistance of the alloy continued to improve with increases in the La content.

Keywords: Al-Fe-Cu alloy; La addition; microstructure; mechanical properties; corrosion behavior



Citation: Xu, Y.; Peng, Z.; Ding, D.; Zhang, W.; Gao, Y.; Chen, G.; Xie, Y.; Liao, Y. Effect of La Addition on Microstructure and Properties of Al-0.2Fe-0.06Cu Alloy. *Metals* **2022**, *12*, 211. <https://doi.org/10.3390/met12020211>

Academic Editor: Akira Otsuki

Received: 6 December 2021

Accepted: 21 January 2022

Published: 24 January 2022

Publisher's Note: MDPI stays neutral with regard to jurisdictional claims in published maps and institutional affiliations.



Copyright: © 2022 by the authors. Licensee MDPI, Basel, Switzerland. This article is an open access article distributed under the terms and conditions of the Creative Commons Attribution (CC BY) license (<https://creativecommons.org/licenses/by/4.0/>).

1. Introduction

Aluminum (Al) is the most abundant metal resource stored in nature, constituting about 8wt.% of the entire crust. Aluminum has three very important advantages: (1) Light weight and high specific strength. The density of aluminum is only $2.7 \times 10^3 \text{ kg}\cdot\text{m}^{-3}$; (2) Good electrical and thermal properties. Its electrical conductivity is about 60% of copper, but if the electrical conductivity is calculated per unit mass, the electrical conductivity of aluminum metal will exceed that of copper; (3) Excellent corrosion resistance. When aluminum is in contact with air, it can quickly react with oxygen in the air, forming a dense Al_2O_3 film on its surface to protect the aluminum inside. These advantages have led to Al foil becoming one of the best choices for lithium-ion battery cathode current collectors.

Owing to many unique features, such as high hardness, low coefficient of friction and average electrical conductivity [1–3], Al-Fe-Cu alloys have several applications. In addition, different micro-alloying elements have different effects on the physical and electrochemical properties of the current collector. Yang et al. [4] reported that the strength and corrosion resistance of the Al-xFe-0.1Si-0.07La ($x = 0.07, 0.2, 0.4\text{wt.}\%$) alloy foil were enhanced as the Fe content increased. Zhu et al. [5] reported that the introduction of La had the effect of refining grains and reducing the quantity of precipitates along the grain boundaries. Additionally, corrosion pits became smaller and fewer when the alloy contained more La. Fe, as one of the main elements of the alloy, can effectively improve heat resistance of aluminum alloys [6,7]. Cu generally exists in the form of a solid solution

state or precipitated state in aluminum alloy, which can increase the strength of the alloy. In addition, different microalloying elements have different effects on the physical and electrochemical properties of the current collector. Addition of La as an alloying element is an effective way to improve the comprehensive properties of aluminum alloys [8–10]. For example, it is beneficial to remove oxygen, hydrogen, sulfur, nitrogen and other impurity elements during the alloy melting process.

Previous studies [11] have reported that adding rare earth compounds to the aluminum solution can significantly reduce the hydrogen content and pinhole ratio. As a good modifier, rare earth can also effectively inhibit the formation of coarse iron-rich phases in aluminum alloys. Furthermore, rare earth elements easily react with alloying elements to form refractory compounds. These refractory compounds can be uniformly dispersed in the aluminum alloy matrix, and work for refining grains and strengthening grain boundaries [12–14]. The rare earth element dissolved in the Al matrix can increase the negative potential of the Al matrix, and the potential will decrease after forming compounds with the rare earth element. Corrosion resistance of the alloy can thus be improved.

Jiang et al. [15] studied the effects of rare earth Ce and La on the microstructure tensile properties and fracture behavior of A357 alloy under as-cast and T6 conditions. They found that the addition of rare earth elements significantly reduced the sizes of the α -Al primary phase and the eutectic Si particles, and improved the morphology of the eutectic Si particles. Yao et al. [16] reported that when La was added to Al–Cu alloy, $\text{Al}_{11}\text{La}_3$ particles were very stable, forming at grain boundaries and effectively suppressing dislocation and grain boundary migration during creep. After 6xxx aluminum alloy was added with La [17], the as-cast properties of the alloy could be improved, which promoted the precipitation of α -AlFeSi phase while suppressing the precipitation of lath-like harmful β phase.

To date, research on the microstructure, mechanical properties and electrochemical properties of Al-0.2Fe-0.06Cu alloy with La content has not been reported. Therefore, the purpose of our investigation is to evaluate the effect of La content on the microstructure and properties of Al-0.2Fe-0.06Cu alloy through microstructural characterization, tensile testing, electrical and electrochemical tests.

2. Materials and Methods

Al-0.2Fe-0.06Cu alloy foils with different La content (i.e., 0wt.% La, 0.1wt.% La and 0.15wt.% La) were used as the experimental materials. All the aluminum alloys used in the experiments were fabricated from pure Al ingot, Al-75wt.% Fe, Al-50wt.% Cu and Al-20wt.% La master alloys. After being melted in the vacuum induction furnace, the aluminum alloy was casted in a metal mold with a size of $350 \times 200 \times 40 \text{ mm}^3$ at 720°C . Then, the aluminum alloy ingots were homogenized at 590°C for 8 h. Finally, the ingots were hot rolled and cold rolled to a thickness of about 0.07 mm. In order to simulate the effect of subsequent pole piece (coated current collector) drying process on the properties of the alloy foils [18], we heat-treated the cold-rolled alloy foils at 120°C for 10 h.

Room temperature tensile test of aluminum foil was performed with the Zwick/Roell Z020 (Zwick Roell Group, Ulm, Germany) electronic universal testing machine. The gauge length of the sample was set to 50 mm and the tensile rate was set to 2 mm/min. CMT 5105 (Meters Testing Machine Factory, Tianjin, China) microcomputer controlled electronic universal testing machine was used for high temperature tensile test (50°C). After the temperature rose to the specified temperature, we hold it for 10 min before starting the tensile test. Tensile rate was set to 2 mm/min. In order to ensure accuracy, at least four parallel samples for each alloy were tested. We used SIGMATEST 2.069 to test alloy conductivity; the test accuracy of this device was 0.01% IACS (International Annealed Copper Standard).

A CHI 660C (Shanghai Chenhua Instrument Company, Shanghai, China) electrochemical workstation was used to test the Tafel polarization curve. The experiment was carried out using a three-electrode system. The working electrode, reference electrode, and counter electrode were the aluminum alloy foil, the saturated calomel electrode and the platinum

wire, respectively. The electrolyte used in the experiment was 3.5wt.% NaCl solution. The voltage range of the Tafel polarization curve test was from -1 V to 0 V, and the scanning speed was 0.001 V/s to obtain accurate electrochemical test results.

The microstructure along the rolling direction was observed with a polarization mode optical microscope (OM, ZEISS imageA1m, Jena, Germany) after mechanical polishing and anodic coating (at 25 V, the mixture of H_3PO_4 , H_2SO_4 and H_2O) of the as-rolled foils and heat-treated foils in stacked form. The phase structure of the alloy was analyzed by X-ray diffractometer (XRD, Rigaku D/max 2500, Tokyo, Japan). The metallographic structure of the aluminum alloy foil was observed with optical microscope (OM, ZEISS imageA1m, Jena, Germany). Secondary phase morphology and distribution of the alloy were observed using scanning electron microscope (SEM, MIRA3, TESCAN, Brno, Czech Republic) in the backscattering mode. At the same time, the composition of the precipitated phase was determined in combination with the energy spectrum diffraction analyzer provided with the scanning electron microscope. The tensile fracture morphology and corroded surface were observed with scanning electron microscope (SEM, VEGA3 (LaB6), TESCAN, Brno, Czech Republic) in secondary electron mode. The chemical composition of the remaining substances in the corrosion pit was analyzed by energy dispersive X-ray spectroscopy (EDS, Aztec X-MaxN80, TESCAN, Brno, Czech Republic).

3. Results and Discussion

3.1. Microstructure

Figure 1 shows a typical metallographic micrograph of the Al-0.2Fe-0.06Cu alloy ingot with different La content after homogenization. The samples had been corroded by Keller reagent (95 mL H_2O , 2.5 mL HNO_3 , 1.5 mL HCl and 1.0 mL HF) to show the grain boundaries. Corresponding higher magnification images revealed that most of the secondary phases tended to precipitate along the grain boundaries of the Al matrix. In the La-free alloy (Figure 1a, Al-0.2Fe-0.06Cu), the grains seemed larger. When La addition was 0.1wt.% (Figure 1b, Al-0.2Fe-0.06Cu-0.1La) and 0.2wt.% (Figure 1c, Al-0.2Fe-0.06Cu-0.15La), the grains became finer. In order to quantitatively compare the grain sizes of alloys with different La content, the software of IPP6.0 (Image Pro Plus 6.0, Media Cybernetics, Rockville, MD, USA) was used to measure the grain size by the intercept method, which evaluated more than 100 grains for each alloy. The statistical results are shown in Table 1. It can be found that the grain size of the La-containing alloy was obviously reduced, and the grain size was the smallest when the La content was 0.1wt.%. The grain refinement should be attributed to the strong chemical activity of La element and heterogeneous nucleation of Al-La compounds of intermediate alloy. During the solidification process of the alloy melt, the La element was easy to gather at the solid-liquid front. It could form an activation film on the surface of the grains, which could inhibit the growth of the grains and be favorable for the grain refinement [12]. For the intermediate alloy of Al-20La, Al-La compounds had a much higher melting temperature and good stability. Thus, in the Al-Fe-La alloy melt, the above Al-La compounds could serve as heterogeneous nucleation points, which helped to refine the grains of the alloy. However, when more La elements were added, the liquid phase composition at the solid-liquid frontier would easily reach the eutectic composition La-containing compounds.

Figure 2 shows longitudinal section microstructures of the foil alloy in different states. Figure 2a–c are metallographic micrographs of different alloys in the cold-rolled state. It can be observed that the grains (slender fibrous structure) of the alloys were stretched and flattened along the rolling direction, showing fibrous tissue. In the La-free alloy (Figure 2a, Al-0.2Fe-0.06Cu), the structure was relatively coarse. When La content was 0.1wt.% (Figure 2b, Al-0.2Fe-0.06Cu-0.1La) and 0.15wt.% (Figure 2c, Al-0.2Fe-0.06Cu-0.15La), the microstructures were significantly refined, and strip-shaped fibrous tissue was tighter. Figure 2d–f are the metallographic micrographs of Al-0.2Fe-0.06Cu alloy with different La addition after heat-treatment of the cold-rolled alloy at 120 °C for 10 h. The

variation of heat-treated alloy microstructure with La content was basically consistent with that of the cold-rolled state.

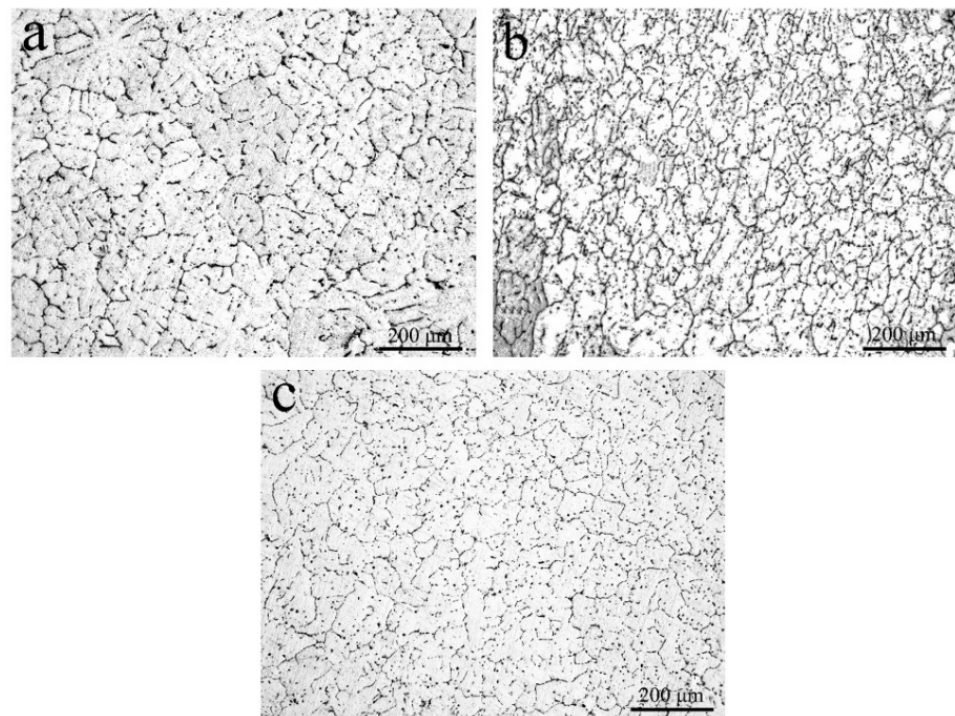


Figure 1. Microstructure of the as-homogenized ingot alloys: (a) Al-0.2Fe-0.06Cu; (b) Al-0.2Fe-0.06Cu-0.1La; (c) Al-0.2Fe-0.06Cu-0.15La.

Table 1. Average grain size of the as-homogenized ingot alloys with different La contents.

Alloy Composition		Al-0.2Fe-0.06Cu		
La content	0wt.% La	0.1wt.% La	0.15wt.% La	
Average grain size (μm)	80.80 ± 5.40	56.64 ± 5.13	60.57 ± 6.41	

Comparing the metallographic images of the foil alloys in different states, it could be found that the microstructure of the alloys did not change much. This indicates that a low temperature heat-treatment process of 120 °C for 10 h had little effect on the microstructure of Al-0.2Fe-0.06Cu alloy with different La addition. In addition, it had been observed that after the rolling process of the alloy, the microstructure still kept the La-induced size effect of the homogenized microstructure because the original grain size seemed to determine the fineness of the as-rolled microstructure.

Figure 3 shows electrical conductivity of the cold-rolled and heat-treated foil alloys with different La additions. The conductivity of the Al-0.2Fe-0.06Cu alloys in different states had little difference. The electrical conductivity of the heat-treated alloys was higher than that of corresponding cold-rolled alloys. This may be due to the motion of dislocation at a given temperature. Under different treatment conditions, the influence of La content on the conductivity was almost the same. As the La content increased from 0wt.% to 0.1wt.%, the conductivity decreased. When the La content increased from 0.1wt.% to 0.15wt.%, the conductivity slightly increased. This was consistent with the change in grain size. This also shows that the grain size had a minor influence on the electrical conductivity, and the decrease in the grain size will reduce the electrical conductivity of the alloy to a certain extent.

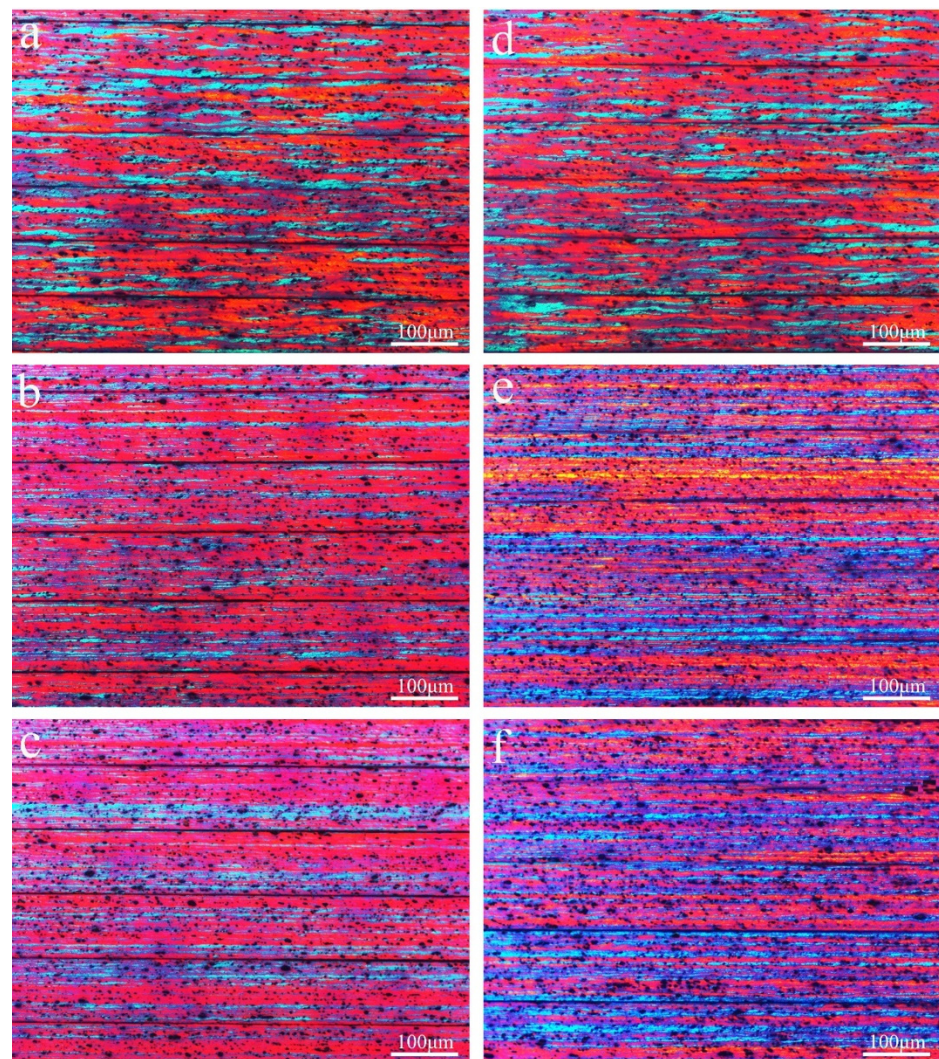


Figure 2. Longitudinal section microstructure of the foil alloys at different states: (a,d) Al-0.2Fe-0.06Cu; (b,e) Al-0.2Fe-0.06Cu-0.1La; (c,f) Al-0.2Fe-0.06Cu-0.15La.

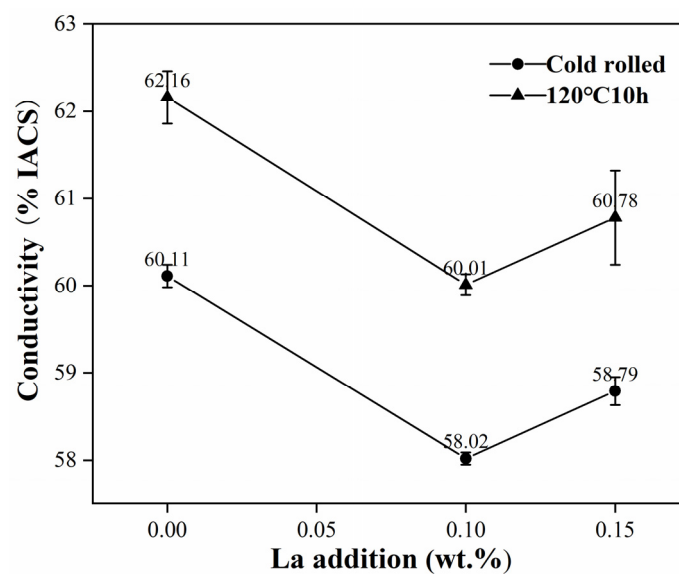


Figure 3. Conductivity of the foil alloys with different La content.

Figure 4 shows X-ray diffraction patterns of the as-homogenized ingot and heat-treated foil alloys. As can be seen in Figure 4, α -Al matrix existed in the alloys with different La content. Compared to the XRD pattern of the as-homogenized alloy, the phase peak strength of α -Al in the heat-treated foil alloys was greatly weakened, and the phase peaks of the second phases almost disappeared, which indicated that during the rolling process, a large number of α -Al matrix and second phases were broken, and their phase peaks were weakened.

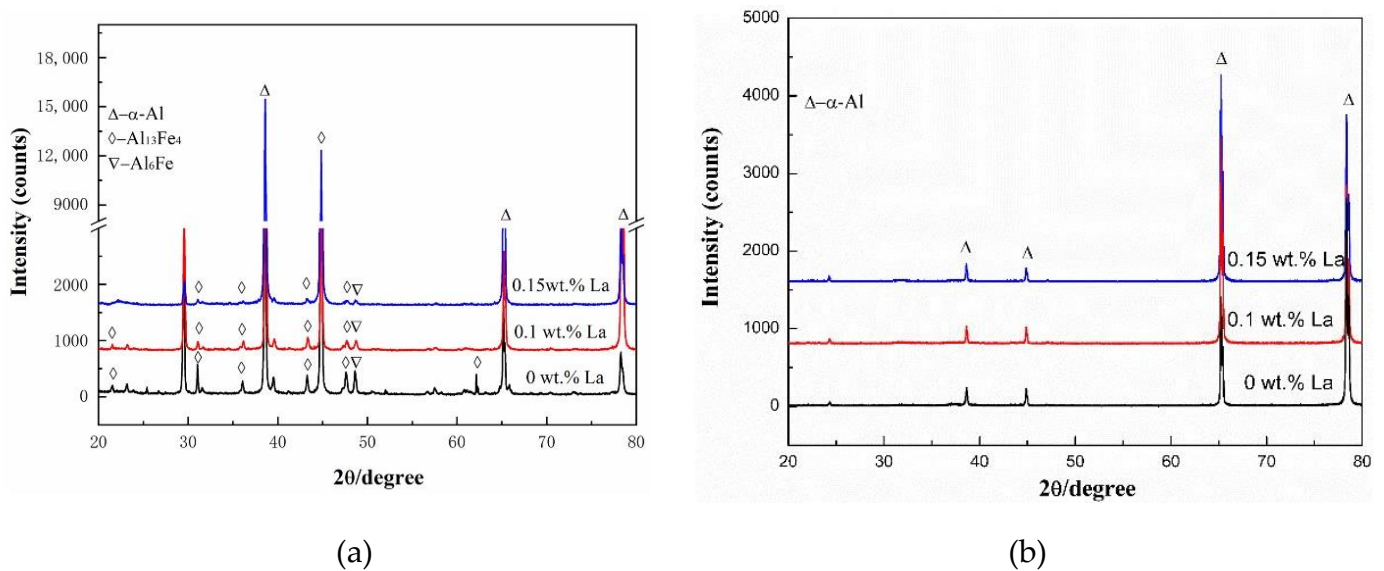


Figure 4. XRD patterns of the alloys: (a) as-homogenized ingot; (b) heat-treated foil.

Figure 5a–c present SEM images of Al-0.2Fe-0.06Cu alloys with different La addition after heat treatment at 120 °C for 10 h. The polished surface was parallel to the rolling direction. There were many micrometer-sized particles dispersed in the Al matrix in the three alloys and their shapes were various, including rod-shaped bars, quadrangles, ellipsoids and irregular shapes. It could be determined through the energy X-ray spectrometer (EDS) patterns (Figure 5d,e) that the particles indicated by the arrow and cross marks in Figure 5a–c were AlFe and AlFeLa phases, respectively. Combined with the testing results of the XRD diffraction pattern (Figure 4), it could be further determined that the AlFe particles were $\text{Al}_{13}\text{Fe}_4$ and Al_6Fe [19–21]. The morphology of particles with different compositions was also different. Most of the AlFe phases had a rod-shape and the size was relatively large. The AlFeLa phases were ellipsoidal and smaller. Compared to the La-free alloy (Figure 5a, Al-0.2Fe-0.06Cu), the AlFeLa phase appeared in the La-containing alloy (Figure 5b, Al-0.2Fe-0.06Cu-0.1La) and the number of AlFe particles was significantly reduced with a smaller size. As the La content increased to 0.15wt.% (Figure 5c, Al-0.2Fe-0.06Cu-0.15La), it was simultaneously observed that the number of AlFeLa phase began to increase. The quantity of AlFe particles was further reduced. With the addition of La, the size of the Al_3Fe phase decreased as the rare earth La had strong chemical properties and was easy to gather around the second phase [4,5].

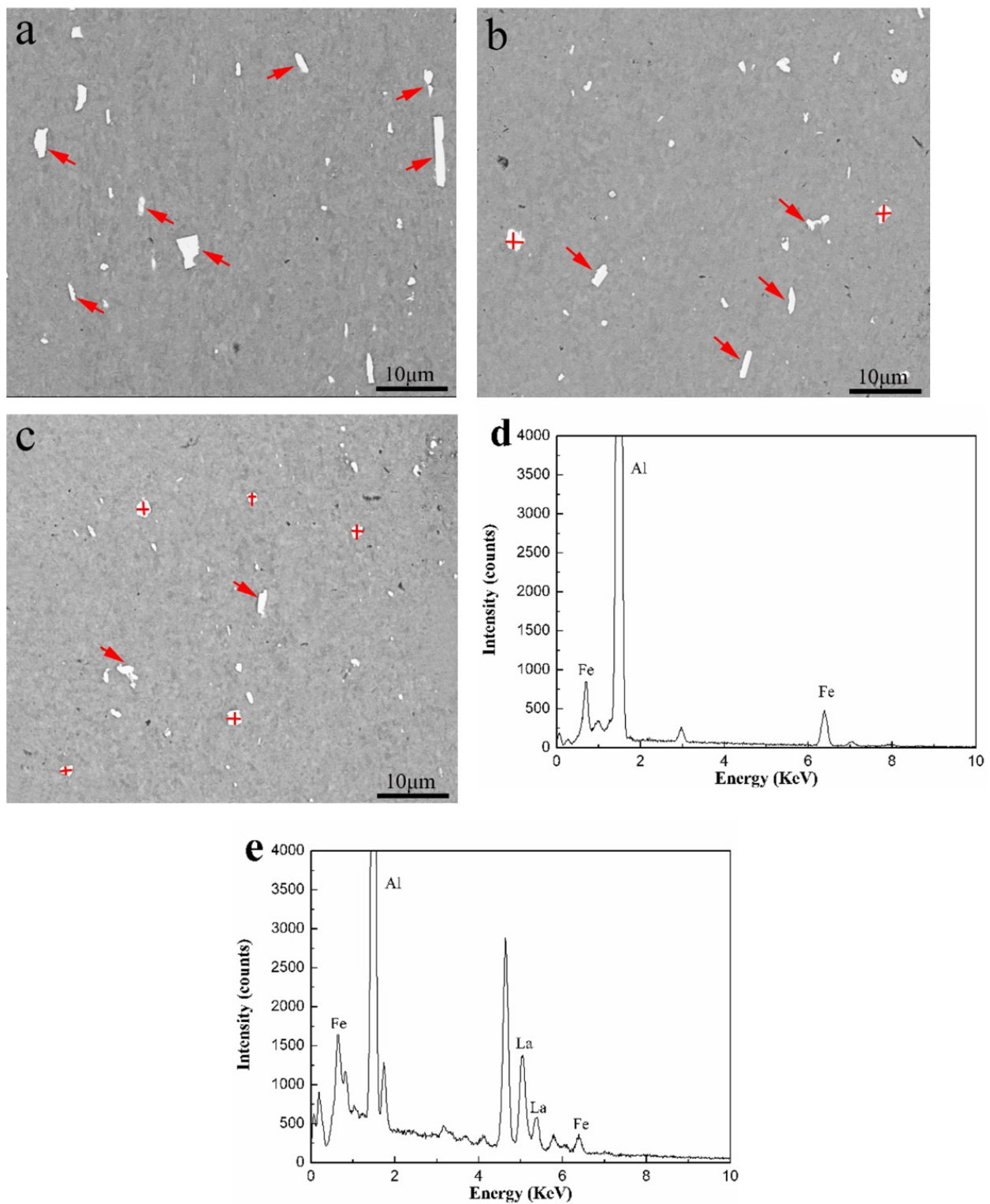


Figure 5. SEM images and energy X-ray spectroscopy patterns of the foil alloys: (a) Al-0.2Fe-0.06Cu; (b) Al-0.2Fe-0.06Cu-0.1La; (c) Al-0.2Fe-0.06Cu-0.15La; (d,e) EDS patterns of AlFe phase (arrow mark) and AlFeLa phase (cross mark).

3.2. Mechanical Properties

Lithium-ion batteries used in terminal equipment can be used in the range of 0 °C to 35 °C. The ideal operating temperature range is 16 °C to 25 °C. Under certain limited conditions, they can be stored between −20 °C and 45 °C [22]. Charging or storing in a high temperature environment may permanently damage the battery capacity and further accelerate the reduction of battery cycle life. Therefore, we simulated the extreme use/storage of current collectors for lithium-ion batteries by subjecting the heat-treated alloys to a high-temperature tensile test at 50 °C. Table 2 lists the room temperature and high temperature tensile properties of the Al-0.2Fe-0.06Cu alloy with different La additions after heat-treatment at 120 °C for 10 h. From Table 2, it can be seen that the tensile strength, yield strength and elongation of alloys under different tensile temperature were close. Both the tensile strength and yield strength decreased, and elongation increased. This could be due to the increase in tensile temperature leading to the thermal activation energy being increased, and the dislocation cross-sliding becoming easier, resulting in a decrease in tensile strength and yield strength. On the other hand, the α -Al matrix softened and the elongation slightly increased [23].

At room temperature, when the La element content was 0wt.%, the tensile strength, yield strength and elongation of the alloy was 202.61 MPa, 190.75 MPa and 1.09%, respectively; when the La content was 0.1wt.%, the tensile strength, yield strength and elongation of the alloy were 220.50 MPa, 208.75 MPa and 1.43%, respectively. Compared to the La-free alloy, the tensile strength increased by 8.83%, the yield strength increased by 7.62% and the elongation increased by 31.19%. When the La content increased from 0.1wt.% to 0.15wt.%, the tensile strength, yield strength and elongation of the alloy slightly decreased. Compared to the 0.1wt.% La addition alloy, the tensile strength decreased by 3.58%, the yield strength decreased by 4.93% and elongation increased by 3.50%. Change of the tensile strength, yield strength and elongation at 50 °C were similar to the tensile results at room temperature. It showed that the addition of La element was beneficial to the improvement of mechanical properties of Al-0.2Fe-0.06Cu alloy. In addition, the degree of grain refinement of the alloy was consistent with the final mechanical property results. The higher the degree of grain refinement, the better the mechanical properties were. This indicated that for the Al-0.2Fe-0.06Cu alloy with different La content, the degree of refinement of the microstructure played a major role in affecting the mechanical properties.

Table 2. Mechanical properties of foil the alloys under different conditions.

Alloy Composition	La Content (wt.%)	σ_b (MPa)		$\sigma_{0.2}$ (MPa)		δ (%)	
		25 °C	50 °C	25 °C	50 °C	25 °C	50 °C
Al-0.2Fe-0.06Cu	0	203 ± 2	191 ± 4	193 ± 1	171 ± 2	1.1 ± 0.1	1.3 ± 0.1
	0.1	221 ± 1	209 ± 2	208 ± 1	181 ± 5	1.4 ± 0.1	1.6 ± 0.1
	0.15	213 ± 1	203 ± 5	198 ± 1	175 ± 5	1.5 ± 0.1	1.6 ± 0.1

Figures 6 and 7 show the fracture surfaces of the alloys under different tensile conditions. Regardless of the tensile temperature, the microscopic morphology of the tensile fracture surface of the alloys was mainly composed of dimples, which belongs to the ductile fracture. The dimples were irregularly shaped and unevenly distributed along a particular direction. Figure 6 shows the tested tensile fracture surface of the alloys at room temperature. A large number of dimples were observed at the tensile fracture surface of the alloys with different La content. With the addition of La, the dimple area tended to become larger. This means that the La addition was beneficial to improve the plasticity of Al-0.2Fe-0.06Cu alloy. In general, fine-grain metals have better plasticity than coarse-grain metals. When fine grains are plastically deformed by external forces, multiple grains are deformed at the same time. The plastic deformation is evenly distributed so that stress concentration does not easily occur, thus yielding better plasticity.

Figure 7 shows the fracture surface of the alloys after the tensile test at 50 °C. The microscopic morphology of the tensile fracture was very similar to that of the room-temperature tensile fracture, i.e., the ductile-dominated fractures with dimples as the main morphology. With the increase in testing temperature, the area of the dimples increased. Comparing Figures 6 and 7, it could be further found that the fracture morphology of the alloy under different tensile conditions was similar. As the testing temperature increased, the number of dimples at the fracture surface increased. Therefore, the plasticity of the alloy was better at 50 °C.

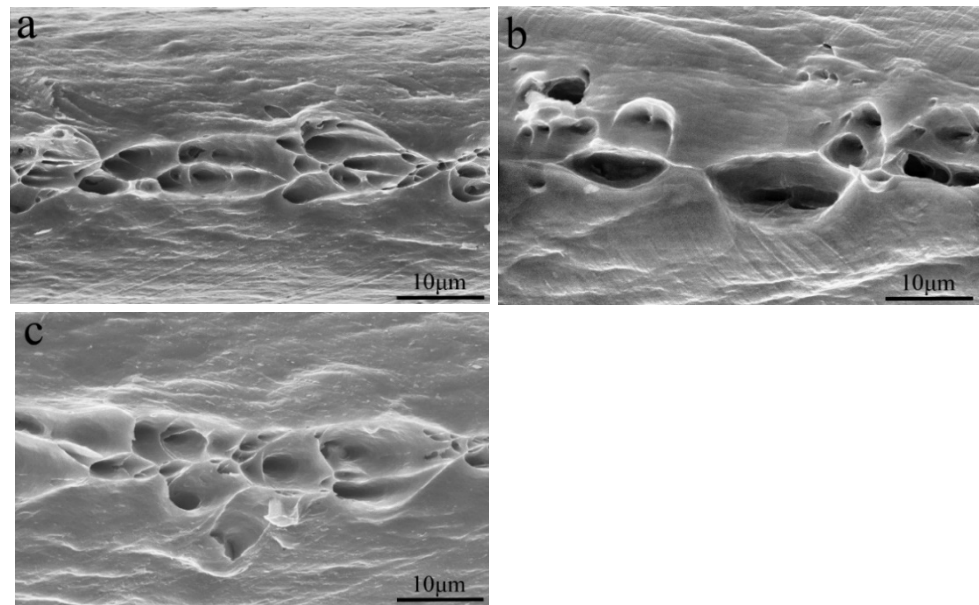


Figure 6. Tensile fracture morphology of the heat-treated foil alloys tested at 25 °C: (a) Al-0.2Fe-0.06Cu; (b) Al-0.2Fe-0.06Cu-0.1La; (c) Al-0.2Fe-0.06Cu-0.15La.

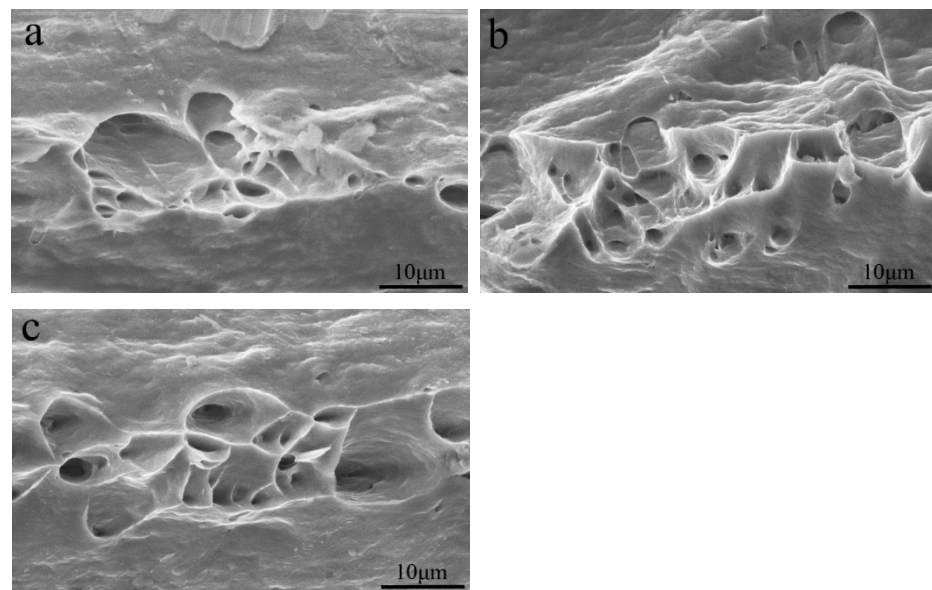


Figure 7. Tensile fracture morphology of the heat-treated foil alloys tested at 50 °C: (a) Al-0.2Fe-0.06Cu; (b) Al-0.2Fe-0.06Cu-0.1La; (c) Al-0.2Fe-0.06Cu-0.15La.

3.3. Electrochemical Performance

Corrosion is the process that slowly, progressively or rapidly damages the appearance, surface or performance of metals under the influence of the surrounding environment, such as atmosphere, water, seawater, different solutions and organic environments [24–27]. Different types of corrosion can occur on the aluminum surface, such as uniform corrosion, pitting corrosion and stress corrosion [28,29]. The form of local corrosion is defined by the formation of irregular corrosion pits on the metal surface [30]. Aluminum is susceptible to pitting corrosion in near-neutral medium environments, which includes almost all natural environments, such as surface moisture, seawater and humid air [31–33]. The process of pitting corrosion can be roughly summarized as the passivation cracks and forms the metastable pit. The pit continues to grow and become the steady state pit [34].

The Tafel polarization curves of the heat-treated alloys in 3.5wt.% NaCl solution were measured to characterize the alloy's electrochemical characteristics. The polarization curve is shown in Figure 8. It can be seen that the shape of the polarization curves of the alloys with different La content had little difference. As the La content increased, the polarization curve shifted to the positive direction. Self-corrosion potential and corrosion current density are two major parameters of electrochemistry. The more positive the self-corrosion potential, the less prone the alloy is to electrochemical corrosion. A smaller corrosion current density means slower corrosion rate when the alloy undergoes electrochemical corrosion [35]. Table 3 shows the electrochemical parameters of the alloys obtained from Tafel polarization curves [36], where E_{corr} and I_{corr} represented the self-corrosion potential and corrosion current density, respectively. It can be seen in Table 3 that, as the La content increased, the alloy's self-corrosion potential became more positive, and the corrosion current density of the alloy became smaller. This indicated that, with the increase in La content, the tendency of electrochemical corrosion of the alloy became weaker, and the rate of electrochemical corrosion of the alloy became slower.

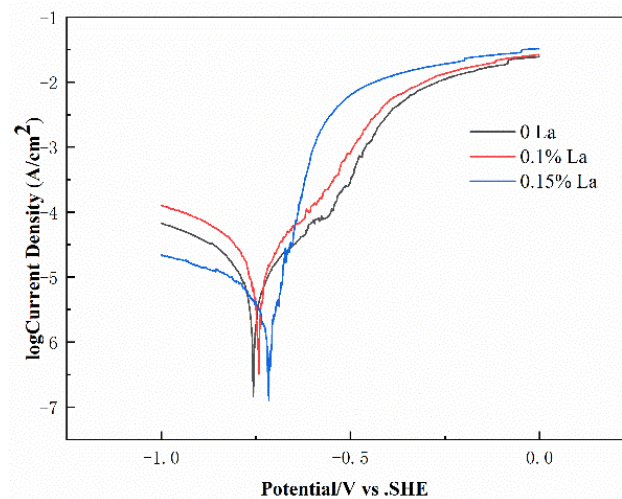


Figure 8. Tafel polarization curves of the alloys with different La content.

Table 3. Electrochemical parameter of the alloys with different La content.

Alloys Composition (wt.%)	La Content (wt.%)	E_{corr} (mV vs. SCE)	I_{corr} (10^{-5} A/cm ²)
Al-0.2Fe-0.06Cu	0	-761 ± 8	1.175
	0.1	-746 ± 3	1.799
	0.15	-723 ± 5	0.478

Figure 9 shows the corroded surfaces of the heat-treated alloys after Tafel testing in the 3.5wt.% NaCl solution. Obviously, corrosion of the presented alloys appeared as pitting of aluminum alloy and further developed into local corrosion. Dimples with similar morphology were observed at the corroded surfaces of the alloys with different La additions. Compared to the La-containing alloys, the La-free alloys had more pits and larger pit areas. When the La content increased from 0.1wt.% to 0.15wt.%, fewer corrosion pits were found in the Al matrix and the distribution of corrosion pits was more dispersed. This was consistent with the Tafel testing results of the electrochemical parameters in Table 3.

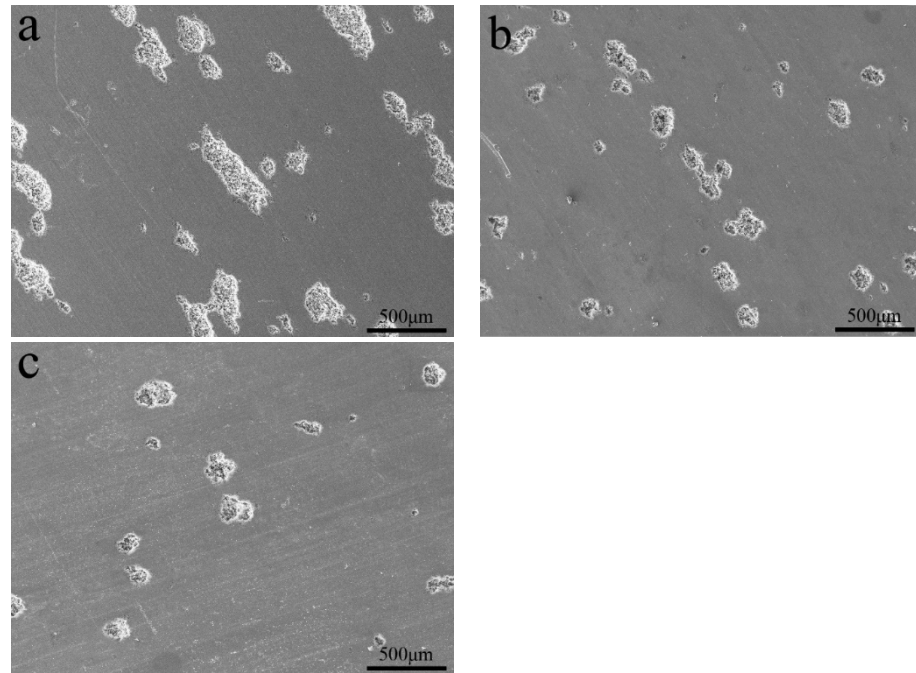


Figure 9. SEM images of corrosion surface of the foil alloys: (a) Al-0.2Fe-0.06Cu; (b) Al-0.2Fe-0.06Cu-0.1La; (c) Al-0.2Fe-0.06Cu-0.15La.

Figure 10 shows high-magnification images of the corrosion surfaces and energy spectrum analysis of residual materials in the corrosion pits. The morphology of the residual material in the corrosion pits of the alloys with different La content was very similar, and the inside of the corrosion pits were all rough microstructures. Combined with EDS analysis, it could be concluded that the residual materials M and N in the pits were the AlFe phase and the AlFeLa phase, respectively. And the area of the pit where the AlFeLa phase was located was smaller. The Fe-rich phase had a high corrosion potential [37], which was the catalytic site of the cathodic reaction and the site of pit nucleation [38]. The La addition was beneficial to improve the corrosion resistance of the Al-0.2Fe-0.06Cu alloy, which was mainly attributed to the following points: (1) The rare-earth elements dissolved in the Al matrix could increase the negative potential of the Al matrix and reduce the Al potential difference between the matrix and the precipitated second phase. (2) Compared to the AlFe compounds, the potential of the AlFeLa compounds was lower, which further reduced the potential difference between the Al matrix and the second phase, and thus improved alloy corrosion resistance. The La addition promoted the formation of the second phase of AlFeLa, while it reduced the number of Al₃Fe in the second phase in the Al matrix. Therefore, the corrosion resistance of the three alloys was improved after the addition of La.

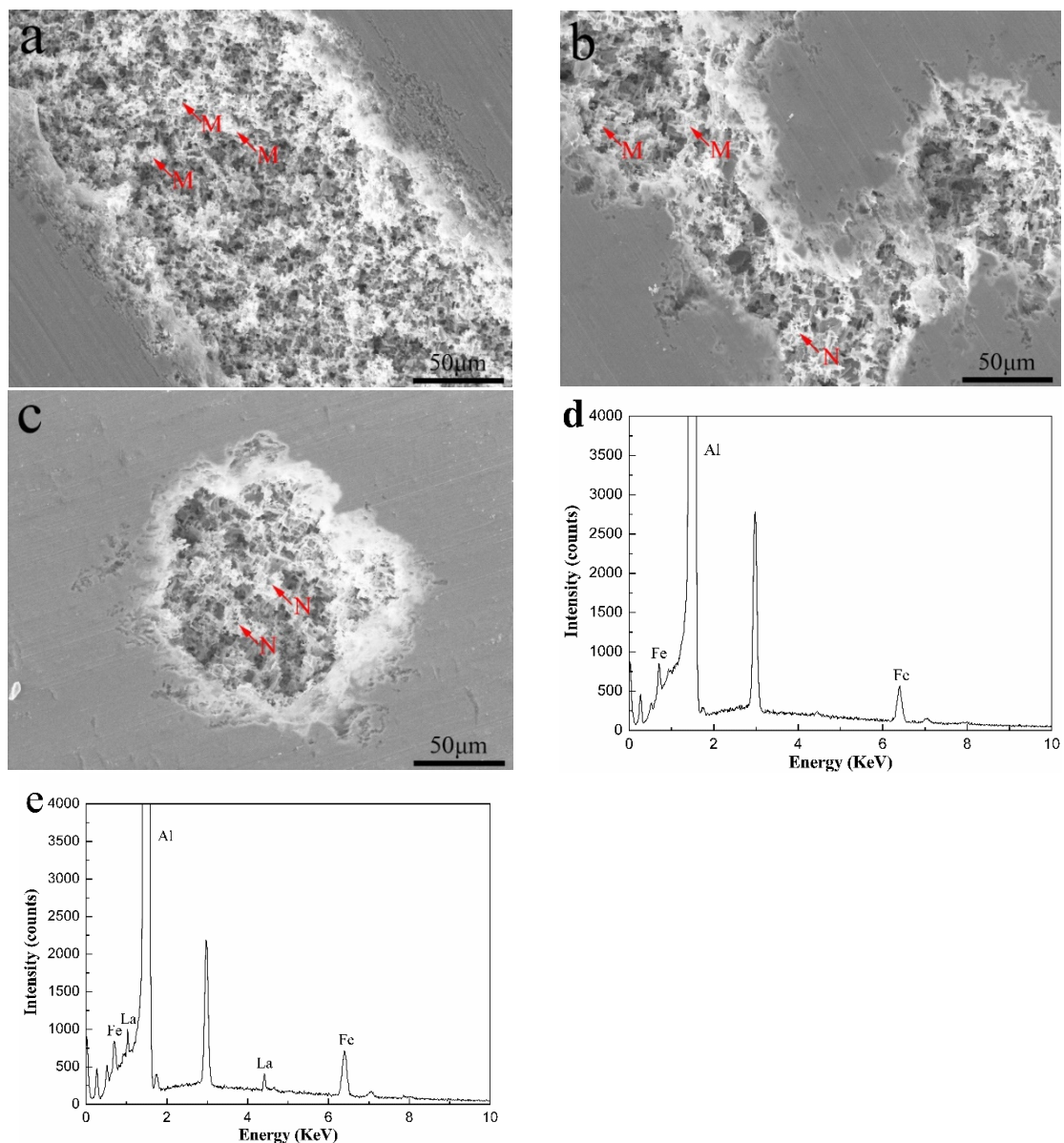


Figure 10. SEM images and energy dispersive X-ray spectroscopy (EDS) patterns of corrosion surface of the alloys: (a) Al-0.2Fe-0.06Cu; (b) Al-0.2Fe-0.06Cu-0.1La; (c) Al-0.2Fe-0.06Cu-0.15La; (d,e) EDS pattern of AlFe particle (M) and AlFeLa particle (N).

4. Conclusions

In this work, the microstructure, mechanical properties and electrochemical properties of Al-0.2Fe-0.06Cu alloys with different La content were systematically investigated. The La addition had the effect of refining grains and reducing the number of precipitates at the grain boundaries. It could be determined through the EDS analysis that the particles were in AlFe and AlFeLa phases, respectively. The electrical conductivity of the heat-treated alloys was higher than that of the corresponding cold-rolled alloys. The fracture morphology of the alloy under different tensile conditions was similar. As the testing temperature increased, the number of dimples at the fracture surface increased.

The electrochemical test reflected the corrosion resistance of the alloy. Compared to the La-containing alloys, the La-free alloys had more pits and larger pit areas. As the La addition increased from 0.1wt.% to 0.15wt.%, fewer corrosion pits were found on the Al matrix and the distribution of corrosion pits was more dispersed. This indicates

that the addition of La element could significantly improve the corrosion resistance of Al-0.2Fe-0.06Cu alloy.

Owing to the high strength, good corrosion resistance and sound electrical conductivity, La-containing Al-Fe-Cu alloys are promising for application as current collectors of lithium-ion batteries.

Author Contributions: Conceptualization, D.D.; formal analysis, W.Z., Y.G., G.C., Y.X. (Yawu Xu), Y.X. (Yonglin Xie) and Y.L.; investigation, Y.X. (Yawu Xu) and Z.P.; writing—original draft preparation, Y.X. (Yawu Xu); writing—review and editing, Y.X. (Yawu Xu) and D.D.; project administration, D.D. All authors have read and agreed to the published version of the manuscript.

Funding: This work was supported by the Shanghai Excellent Technical Leader Project (No. 15XD1524600).

Data Availability Statement: Not applicable.

Acknowledgments: The authors would like to thank the Instrumental Analysis Center of Shanghai Jiao Tong University for SEM experiments.

Conflicts of Interest: The authors declare no conflict of interest.

References

1. Köster, U.; Liu, W.; Liebertz, H.; Michel, M. Mechanical properties of quasicrystalline and crystalline phases in Al-Cu-Fe alloys. *J. Non-Cryst. Solids* **1993**, *153–154*, 446–452. [[CrossRef](#)]
2. Köster, U.; Liebertz, H.; Liu, W. Plastic deformation of quasi-crystalline and crystalline phases in Al-Cu-Fe alloys. *Mater. Sci. Eng. A* **1994**, *181–182*, 777–780. [[CrossRef](#)]
3. Bilušić, A.; Pavuna, D.; Smontara, A. Figure of merit of quasicrystals: The case of Al-Cu-Fe. *Vacuum* **2001**, *61*, 345–348. [[CrossRef](#)]
4. Yang, X.; Ding, D.; Xu, Y.; Zhang, W. Al-Fe-Si-La alloys for current collectors of positive electrodes in lithium ion batteries. *Metals* **2020**, *10*, 109. [[CrossRef](#)]
5. Zhu, J.; Ding, D.; Zhang, W. Effect of La addition on the microstructure and properties of Al-Fe-Mn alloys for lithium battery current collectors. *J. Electron. Mater.* **2021**, *50*, 1032–1043. [[CrossRef](#)]
6. Couture, A. Iron in aluminium casting alloys—a literature survey. *AFS Inter. Cast. Met.* **1981**, *12*, 9–17.
7. Stefaniay, V.; Criger, A.; Turmezey, T. Intermetallic phases in the aluminum-side corner of the AlFeSi alloy system. *J. Mater. Sci.* **1987**, *23*, 539–546. [[CrossRef](#)]
8. Nie, Z.R.; Jin, T.; Fu, J.; Xu, G.; Yang, J.; Zhou, J.X.; Zuo, T. Research on rare earth in aluminum. *Mater. Sci. Forum* **2002**, *396*, 1731–1735. [[CrossRef](#)]
9. Yao, D.; Xia, Y.; Qiu, F.; Jiang, Q. Effects of La addition on the elevated temperature properties of the casting Al-Cu alloy. *Mater. Sci. Eng. A* **2011**, *528*, 1463–1466. [[CrossRef](#)]
10. Zhang, X.; Xiong, J.; Zhao, G.; Lai, R.; Wu, Y. Effect of rare earth La on microstructures and ageing characteristics of 6063 aluminum alloy. *Trans. Nonferrous Met. Soc. China* **2020**, *62*, 1–5.
11. Gschneidner, K.A. Rare earth alloys: A critical review of the alloy systems of the rare earth, scandium, and yttrium metals. *J. Am. Chem. Soc.* **1962**, *84*, 123.
12. Chen, Y.; Pan, Y.; Lu, T.; Tao, S.; Wu, J. Effects of combinative addition of lanthanum and boron on grain refinement of Al-Si casting alloys. *Mater. Des.* **2014**, *64*, 423–426. [[CrossRef](#)]
13. Chang, J.Y.; Kim, G.H.; Moon, I.G.; Choi, C.S. Rare earth concentration in the primary Si crystal in rare earth added Al-21wt.%Si alloy. *Scr. Mater.* **1998**, *39*, 307–314. [[CrossRef](#)]
14. Chang, J.; Moon, I.; Choi, C. Refinement of cast microstructure of hypereutectic Al-Si alloys through the addition of rare earth metals. *J. Mater. Sci.* **1998**, *33*, 5015–5023. [[CrossRef](#)]
15. Jiang, W.; Fan, Z.; Dai, Y.; Li, C. Effects of rare earth elements addition on microstructures, tensile properties and fractography of A357 alloy. *Mater. Sci. Eng. A Struct. Mater. Prop. Microstruct. Process.* **2014**, *597*, 237–244. [[CrossRef](#)]
16. Yao, D.; Zhao, W.; Zhao, H.; Qiu, F.; Jiang, Q. High creep resistance behavior of the casting Al-Cu alloy modified by La. *Scr. Mater.* **2009**, *61*, 1153–1155. [[CrossRef](#)]
17. Hosseinfar, M.; Malakhov, D.V. Effect of Ce and La on microstructure and properties of a 6xxx series type aluminum alloy. *J. Mater. Sci.* **2008**, *43*, 7157–7164. [[CrossRef](#)]
18. Westphal, B.; Bockholt, H.; Günther, T.; Haselrieder, W.; Kwade, A. Influence of convective drying parameters on electrode performance and physical electrode properties. *ECS Trans.* **2015**, *64*, 57–68. [[CrossRef](#)]
19. Gu, J.; Gu, S.; Xue, L. Microstructure and mechanical properties of in-situ Al₁₃Fe₄/Al composites prepared by mechanical alloying and spark plasma sintering. *Mater. Sci. Eng. A* **2012**, *558*, 684–691. [[CrossRef](#)]
20. Kim, D.H.; Cantor, R.; Lee, H.I. Structure and decomposition behavior of rapidly solidified Al-Cu-Li-Mg-Zr alloys. *J. Mater. Sci.* **1988**, *23*, 1695–1708. [[CrossRef](#)]

21. Kim, D.H.; Cantor, B. Quasicrystalline and related crystalline phases in rapidly solidified Al-Fe alloys. *Philos. Mag. A* **1993**, *69*, 45–55. [[CrossRef](#)]
22. Väyrynen, A.; Salminen, J. Lithium ion battery production. *J. Chem. Thermodyn.* **2012**, *46*, 80–85. [[CrossRef](#)]
23. Han, L.; Sui, Y.; Wang, Q.; Wang, K.; Jiang, Y. Effects of Nd on microstructure and mechanical properties of cast Al-Si-Cu-Ni-Mg piston alloys. *J. Alloys Compd.* **2016**, *695*, 1566–1572. [[CrossRef](#)]
24. Aballe, A.; Bethencourt, M.; Botana, F.J.; Marcos, M.; Sánchez-Amaya, J.M. Influence of the degree of polishing of alloy AA 5083 on its behavior against localised alkaline corrosion. *Corros. Sci.* **2004**, *46*, 1909–1920. [[CrossRef](#)]
25. Zaid, B.; Saidi, D.; Benzaid, A.; Hadji, S. Effects of pH and chloride concentration on pitting corrosion of AA6061 aluminum alloy. *Corros. Sci.* **2008**, *50*, 1841–1847. [[CrossRef](#)]
26. Alavi, A.; Cottis, R.A. The determination of pH, potential and chloride concentration in corroding crevices on 304 stainless steel and 7475 aluminium alloy. *Corros. Sci.* **1987**, *27*, 443–451. [[CrossRef](#)]
27. Birbilis, N.; Buchheit, R.G. Investigation and discussion of characteristics for intermetallic phases common to aluminum alloys as a function of solution pH. *J. Electrochem. Soc.* **2008**, *155*, C117–C126. [[CrossRef](#)]
28. Tabrizi, M.R.; Lyon, S.B.; Thompson, G.E. The long-term corrosion of aluminium in alkaline media. *Corros. Sci.* **1991**, *32*, 733–742. [[CrossRef](#)]
29. Aballe, A.; Bethencourt, M.; Botana, F.J.; Cano, M.J.; Marcos, M. Localized alkaline corrosion of alloy AA5083 in neutral 3.5% NaCl solution. *Corros. Sci.* **2001**, *43*, 1657–1674. [[CrossRef](#)]
30. Reboul, M.C.; Warner, T.J.; Mayer, H. A ten step mechanism for the pitting corrosion of aluminium alloys. *Corros. Rev.* **1997**, *15*, 471–496. [[CrossRef](#)]
31. Bogar, F.D.; Foley, R.T. The influence of chloride ion on the pitting of aluminum. *J. Electrochem. Soc.* **1972**, *119*, 462–464. [[CrossRef](#)]
32. Brown, R.H.; Mears, R.B. The electrochemistry of corrosion. *Trans. Electrochem. Soc.* **1938**, *74*, 495. [[CrossRef](#)]
33. Godard, H.P. The corrosion behavior of aluminum in natural waters. *Can. J. Chem. Eng.* **1960**, *38*, 167–173. [[CrossRef](#)]
34. Szklarska-Smialowska, Z. Pitting corrosion of aluminum. *Corros. Sci.* **1999**, *41*, 1743–1767. [[CrossRef](#)]
35. Chai, Z.; Jiang, C.; Zhu, K.; Zhao, Y.; Wang, C.; Cai, F.; Chen, M.; Wang, L. Pretreatment behaviors and improved corrosion resistance for Cu/Co-Ni-Cu coating electrodeposition on magnesium alloy. *J. Electrochem. Soc.* **2016**, *163*, D493–D499. [[CrossRef](#)]
36. Thiede, V.M.T.; Ebel, T.; Jeitschko, W. Ternary aluminides LnT₂Al₁₀ (Ln = Y, La–Nd, Sm, Gd–Lu and T = Fe, Ru, Os) with YbFe₂Al₁₀ type structure and magnetic properties of the iron-containing series. *J. Mater. Chem.* **1998**, *8*, 125–130. [[CrossRef](#)]
37. Rynders, R.M.; Paik, C.H.; Ke, R. Use of in situ atomic force microscopy to image corrosion at inclusions. *J. Electrochem. Soc.* **1994**, *141*, 1439–1445. [[CrossRef](#)]
38. Speckert, L.; Burstein, G.T. Combined anodic/cathodic transient currents within nucleating pits on Al-Fe alloy surfaces. *Corros. Sci.* **2011**, *53*, 534–539. [[CrossRef](#)]